



Prediction of Cardiac Resynchronization Therapy Response Using a Lead Placement Score Derived From 4-Dimensional Computed Tomography

Ashish Manohar¹, PhD; Gabrielle M. Colvert, PhD; James Yang², BS; Zhennong Chen³, PhD; Maria J. Ledesma-Carbayo, PhD; Mads Brix Kronborg⁴, MD, PhD; Anders Sommer, MD, PhD; Bjarne L. Nørgaard, MD, PhD; Jens Cosedis Nielsen⁵, MD, PhD; Elliot R. McVeigh⁶, PhD

BACKGROUND: Cardiac resynchronization therapy (CRT) is an effective treatment for patients with heart failure; however, 30% of patients do not respond to the treatment. We sought to derive patient-specific left ventricle maps of lead placement scores (LPS) that highlight target pacing lead sites for achieving a higher probability of CRT response.

METHODS: Eighty-two subjects recruited for the ImagingCRT trial (Empiric Versus Imaging Guided Left Ventricular Lead Placement in Cardiac Resynchronization Therapy) were retrospectively analyzed. All 82 subjects had 2 contrast-enhanced full cardiac cycle 4-dimensional computed tomography scans: a baseline and a 6-month follow-up scan. CRT response was defined as a reduction in computed tomography–derived end-systolic volume $\geq 15\%$. Eight left ventricle features derived from the baseline scans were used to train a support vector machine via a bagging approach. An LPS map over the left ventricle was created for each subject as a linear combination of the support vector machine feature weights and the subject's own feature vector. Performance for distinguishing responders was performed on the original 82 subjects.

RESULTS: Fifty-two (63%) subjects were responders. Subjects with an $LPS \leq Q_1$ (lower-quartile) had a posttest probability of responding of 14% (3/21), while subjects with an $LPS \geq Q_3$ (upper-quartile) had a posttest probability of responding of 90% (19/21). Subjects with $Q_1 < LPS < Q_3$ had a posttest probability of responding that was essentially unchanged from the pretest probability (75% versus 63%, $P=0.2$). An LPS threshold that maximized the geometric mean of true-negative and true-positive rates identified 26/30 of the nonresponders. The area under the curve of the receiver operating characteristic curve for identifying responders with an LPS threshold was 87%.

CONCLUSIONS: An LPS map was defined using 4-dimensional computed tomography–derived features of left ventricular mechanics. The LPS correlated with CRT response, reclassifying 25% of the subjects into low probability of response, 25% into high probability of response, and 50% unchanged. These encouraging results highlight the potential utility of 4-dimensional computed tomography in guiding patient selection for CRT. The present findings need verification in larger independent data sets and prospective trials.

Key Words: cardiac imaging techniques ■ cardiac resynchronization therapy ■ four-dimensional computed tomography ■ heart failure ■ heart function tests ■ support vector machine ■ ventricular function

Multiple trials have proven that cardiac resynchronization therapy (CRT) can provide significant benefit for patients with intraventricular dyssynchrony and heart failure¹; however, approximately 30% do not respond.²

Significant effort has been focused to reduce the nonresponder rate using echocardiography³; 2-dimensional radial strain from speckle-tracking has been used to identify optimal left ventricle (LV) lead placement,⁴ and

Correspondence to: Elliot R. McVeigh, PhD, Department of Bioengineering, University of California San Diego, 9500 Gilman Dr, Mail Code: 0412, La Jolla, CA. Email emcveigh@ucsd.edu

Supplemental Material is available at <https://www.ahajournals.org/doi/suppl/10.1161/CIRCIMAGING.122.014165>.

Continuing medical education (CME) credit is available for this article. Go to <http://cme.ahajournals.org> to take the quiz.

For Sources of Funding and Disclosures, see page 611.

© 2022 American Heart Association, Inc.

Circulation: Cardiovascular Imaging is available at www.ahajournals.org/journal/circimaging

CLINICAL PERSPECTIVE

Cardiac resynchronization therapy (CRT) is a proven treatment for patients with heart failure and dyssynchrony. However, approximately 30% of patients do not respond; thus, more accurate patient selection for CRT remains an unmet need. Results from image-guided CRT studies have been ambiguous. Poor reproducibility of echocardiography coupled with the complexity of cardiac magnetic resonance have likely contributed to the poor overall adoption of these methods for pre-CRT assessment. In this work, we describe a metric called the lead placement score that combines multiple 4-dimensional computed tomography–derived features of left ventricular mechanics into a single number for each possible pacing lead location on the left ventricle; the features included in the lead placement score map have previously been shown to correlate with CRT response. Using a machine learning classifier, a model was constructed with these features and then used to derive the lead placement score map for each individual subject. The lead placement score correlated with the probability of a subject responding to CRT. Low-dose 4-dimensional computed tomography is now widely available and provides high-resolution images of the full cardiac cycle. The advantages of 4-dimensional computed tomography coupled with the promising results reported in this study, highlight the potential utility of 4-dimensional computed tomography in the planning of CRT.

Nonstandard Abbreviations and Acronyms

4DCT	4-dimensional computed tomography
CMR	cardiac magnetic resonance
CRT	cardiac resynchronization therapy
LPS	lead placement score
LV	left ventricle
LVEF	left ventricular ejection fraction
NYHA	New York Heart Association
SVM	support vector machine

studies have explored tissue doppler imaging in patient selection for CRT.⁵ However, poor reproducibility of echocardiography measurements due to interobserver and intraobserver variability coupled with intervener differences have led to disappointing results and hindered its routine clinical use.⁶

Cardiac magnetic resonance (CMR) imaging has also been used to guide CRT.⁷ Cine magnetic resonance imaging (MRI),⁸ tagged MRI,⁹ and cine displacement encoding with stimulated echoes¹⁰ have shown promise in mapping regional strain and mechanical activation times of the LV myocardium. Also, late gadolinium enhancement imaging can identify regions of scar tissue

to be avoided during lead placement.¹¹ However, 28% of patients under consideration for CRT have existing right ventricular pacing systems¹²; therefore, in patients with non-MRI compatible devices or those without access to advanced imaging centers, MRI will not be available. Additionally, tagged MRI and cine displacement encoding with stimulated echoes images are not simple to acquire and analyze, requiring skilled technicians and image analysis personnel. No imaging modality is currently recommended for CRT planning and management.

Recent studies have explored the use of 4-dimensional computed tomography (4DCT) to guide CRT. Truong et al¹³ used dual-source computed tomography (CT) to derive LV dyssynchrony indices that predicted 2-year major adverse cardiac events. They reported that leads placed on sites with maximal wall thickness correlated with less major adverse cardiac events. Rinaldi et al^{14,15} utilized 4DCT-derived assessment of LV dyssynchrony and myocardial scar to target LV lead placement. They showed that patients with leads implanted in segments targeted from CT had higher clinical response rates¹⁴ and superior acute hemodynamic responses¹⁵ than those with leads implanted in the nontarget segments. Fyenbo et al¹⁶ used CT to identify regions of myocardial scar and to compute scar burden. They found that high scar burden and proximity of scar to the LV pacing site were correlated with echocardiographic nonresponse.

We hoped to improve on the insights from these previous studies by using additional features of LV mechanics that have previously been shown to correlate with CRT response¹ in a larger number of subjects. Thus, the purpose of this study was to use a combination of 4DCT-derived regional and global features of LV mechanics to define patient-specific maps of lead placement scores (LPS) that are correlated with CRT response.

METHODS

The data that support the findings of this study are available from the corresponding author upon reasonable request.

Subject Population and CT Imaging

Subjects recruited for the ImagingCRT¹⁷ (Empiric Versus Imaging Guided Left Ventricular Lead Placement in Cardiac Resynchronization Therapy) randomized controlled trial were retrospectively used for this study. The trial enrolled a total of 182 subjects; 147 subjects had contrast-enhanced 4DCT scans both before and after CRT implantation. The complete study protocol for the trial is described by Sommer et al.^{17,18} The trial was conducted at Aarhus University Hospital, Skejby, Denmark and was approved by the Central Denmark regional committee on health research ethics and the Danish Data Protection Agency. All trial participants gave informed written consent, and the trial was registered on <https://www.clinicaltrials.gov> (Unique identifier: NCT01323686).

The prescribed cardiac 4DCT imaging protocol has previously been described in detail¹⁷ and is described in the Methods sections in the [Supplemental Information](#). Each

subject had 2 contrast-enhanced full cardiac cycle and full LV volume retrospective ECG-gated 4DCT scans: the first scan was on the day before CRT implantation and the second scan was 6 months after implantation; we refer to these scans hereafter as the baseline and the follow-up scans, respectively.

Subjects were excluded from this study if their baseline or follow-up scans had ≥ 1 of the following imaging artifacts, preventing precise measurements of LV mechanics:

1. Severe helical step artifact.
2. Insufficient LV chamber-myocardium contrast for blood volume segmentation.
3. Severe metal artifacts from the pacemaker/defibrillator leads preventing segmentation of the LV blood volume.

LV Segmentation

The LV blood pool was segmented from each reconstructed time frame of the baseline and follow-up 4DCT datasets of each subject. The segmentation procedure employed has previously been described in detail.^{19,20} Additionally, the positions of the right and the left lead tips were marked in the end-diastolic image of the follow-up scans and were used to project the corresponding right and left pacing sites onto the LV endocardial model, respectively (see Figure 1)

Global and Regional Features of LV Mechanics

Eight global and regional features of LV mechanics were derived from the baseline 4DCT scans for each subject. The global LV features used were

1. End-diastolic volume (EDV)
2. End-systolic volume (ESV)
3. Circumferential uniformity ratio estimate using singular value decomposition (CURE-SVD)
4. LV sphericity index (LVSI)

and the regional LV features used were

1. Peak regional shortening (PRS_{CT})
2. Time to peak regional shortening ($TPRS_{CT}$)
3. Maximum prestretch of regional shortening ($MSRS_{CT}$)
4. Time to onset of shortening (TOS)

The choice of these 8 features was driven by previous CRT studies using CMR and CT imaging.^{1,8} Detailed information on the computation of the above 8 features can be found in

the Methods sections in the [Supplemental Material](#). Figure S1 describes the estimation of the 4 regional LV features.

Spatial Sampling of the LV Endocardium

The LV endocardium for each subject was divided into 90 spatial segments: 18 circumferential segments (one every 20°) for each slice, and 5 slices defined from apex to base along the long axis of the LV.¹⁹ This 90-segment model has higher spatial sampling than the American Heart Association 17-segment model, permitting wall function analysis that captures the high-resolution features of mechanical function that are obvious in the 4DCT data. The location of the right and the left lead tips were mapped onto the LV endocardial segments closest to the lead locations. The 4 regional features listed above were estimated for each of these 90 endocardial segments.

Definition of CRT Response

Subjects were considered responders if their CT-derived ESV decreased by $\geq 15\%$ 6 months post-CRT implantation.⁶ The ESV of the subjects were computed from the 4DCT exams as described in the Methods sections in the [Supplemental Material](#), and the change in ESV 6 months postimplantation was calculated between the baseline and the follow-up 4DCT scans.

Lead Placement Score

The LPS is a model that combines the 8 features of baseline LV mechanics listed above into a single scalar value for each endocardial segment, yielding high-resolution LPS maps over the entire LV. Our goal was to derive an LPS that is correlated with CRT response.

The LPS model comprised the following features derived from the baseline 4DCT scan: the global LV features of (1) end-diastolic volume, (2) ESV, (3) circumferential uniformity ratio estimate using singular value decomposition, and (4) LV sphericity index, and the regional LV features of (5) peak regional shortening, (6) time to peak regional shortening, (7) maximum prestretch of regional shortening, and (8) time to onset of shortening. Values at 2 endocardial segments for each of the 4 regional features were used in the model: one at the site of the right lead and the other at the site of the left lead; thus, the model had 12 parameters in total (4 global LV features+4 \times 2 regional LV features). Since all subjects used in this study had

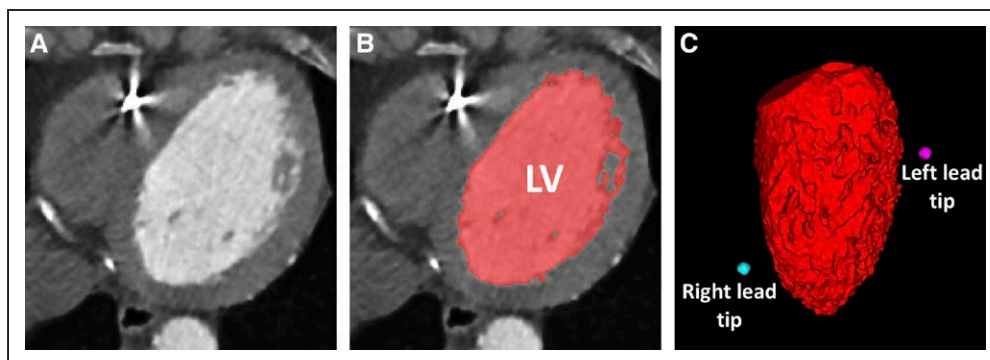


Figure 1. Left ventricle (LV) blood volume segmentation.

A, Axial contrast-enhanced cardiac computed tomography image. **B**, LV blood volume segmentation overlaid in red. **C**, 3-dimensional rendering of the LV blood volume segmentation with the locations of the right (cyan) and the left (magenta) lead tips. The anterior wall is in view with the septum on the left and the lateral wall on the right.

follow-up 4DCT scans, their response states and left and right lead tip locations were precisely known. Hence, for training the model, the 4 regional LV features were estimated from the baseline scans at the two endocardial segments that corresponded to the implanted lead tip locations measured in the follow-up scans. A support vector machine (SVM)²¹ was used for training the LPS model to predict the measured response. Detailed information on the SVM training and the LPS calculation can be found in the Methods sections in the [Supplemental Material](#).

The performance of the trained model was tested on the original cohort of 82 subjects. Additionally, using the trained model, high-resolution LPS maps over the entire LV free wall (anterior wall to inferior wall) were created for each of the 82 subjects. By fixing the right lead location, regional features estimated at all free wall segments were used to create LPS maps highlighting target left lead placement sites for achieving a higher probability of response.

Statistical Analysis

Continuous variables were expressed as mean \pm 1 SD, unless specified otherwise. Categorical variables were expressed as numbers and percentages. Two-sample *t* test for a continuous variable and Fisher's exact test for a categorical variable were conducted for comparing statistically significant difference between the two groups; a *P*<0.05 was considered statistically significant (Table 1).

A linear regression model was fit to assess the association between CT- and echocardiography-derived LV ejection fractions (LVEFs), and the Pearson correlation coefficient was calculated to describe their correlation.

An SVM including 12 CT-derived features of LV mechanics was used to define the LPS, which in turn was used to assess the relationship between the CT-derived features and CRT response (change in ESV at 6 months). The optimal LPS threshold was defined as the value that maximized the geometric mean (*g*-mean) of true-positive and true-negative rates. Subjects with an LPS value greater than the threshold were considered LPS responders, and subjects with an LPS value less than the threshold were considered LPS nonresponders. The true responders were defined as patients in whom Δ ESV \leq -15% after 6 months, and nonresponders were determined using the Δ ESV $>$ -15% after 6 months. The relationship between Δ ESV and LPS was investigated as categorical variables after applying the respective thresholds using Fisher's exact test (Figure 3).

Receiver operating characteristic curves were used to evaluate the performance of the trained SVM models, with their areas under the curve and 95% CIs around the area under the curve estimates reported.

RESULTS

Study Population

Out of the 147 subjects that had both baseline and follow-up 4DCT scans, 82 subjects had images that were of sufficient quality for this study. Scans were excluded because of either helical step artifacts (37 subjects, 25%), insufficient LV blood pool-myocardium contrast (19 subjects, 13%), or severe metallic lead artifacts (9 subjects, 6%). Figure 2 shows a flow

Table 1. Baseline Characteristics of the 82 Subjects

	Total (n=82)	Responder (n=52)	Non-responder (n=30)	<i>P</i> value
Female, n (%)	17 (21)	15 (29)	2 (7)	0.023*
Age, y, mean \pm SD	70.7 \pm 9.1	70.9 \pm 9.4	70.3 \pm 8.7	0.746†
Body mass index, kg/m ² , mean \pm SD	26.5 \pm 4.2	25.9 \pm 4.3	27.7 \pm 3.6	0.054†
6-minute walk test, m, mean \pm SD	393 \pm 124	393 \pm 109	392 \pm 147	0.981†
QRS width (ms), mean \pm SD	170 \pm 24	173 \pm 20	163 \pm 29	0.064†
LBBB, n (%)	77 (94)	47 (90)	30 (100)	0.153*
Chronic RV pacing, n (%)	16 (20)	9 (17)	7 (23)	0.569*
eGFR, mL/min per 1.73 m ² , mean \pm SD	66 \pm 16	65 \pm 16	68 \pm 14	0.316†
Medical history, n (%)				
Hypertension	20 (24)	11 (21)	9 (30)	0.428*
Diabetes	18 (22)	10 (19)	8 (27)	0.58*
Ischemic cardiomyopathy	42 (51)	22 (42)	20 (67)	0.041*
Myocardial infarction	28 (34)	13 (25)	15 (50)	0.03*
CABG	19 (23)	8 (15)	11 (37)	0.034*
NYHA class, n (%)				
II	41 (50)	23 (44)	18 (60)	0.276*
III	39 (48)	28 (54)	11 (37)	
IV	2 (2)	1 (2)	1 (3)	
Atrial fibrillation, n (%)				
Paroxysmal	12 (15)	8 (15)	4 (13)	1*
Permanent	9 (11)	6 (12)	3 (10)	1*
Medicine, n (%)				
β -blockers	75 (91)	48 (92)	27 (90)	0.703*
ACE inhibitor/ARB	78 (95)	49 (94)	29 (97)	1*
Loop diuretics	51 (62)	34 (65)	17 (57)	0.483*
Spironolactone	40 (49)	25 (48)	15 (50)	1*
CT				
EDV, mL, mean \pm SD	273 \pm 93	278 \pm 94	264 \pm 92	0.527†
ESV, mL, mean \pm SD	178 \pm 81	179 \pm 78	177 \pm 87	0.888†
EF (%), mean \pm SD	37 \pm 9	37 \pm 8	36 \pm 11	0.602†
Echocardiography				
EDV, mL, mean \pm SD	257 \pm 85	260 \pm 79	253 \pm 94	0.735†
ESV, mL, mean \pm SD	195 \pm 71	195 \pm 65	193 \pm 80	0.896†
EF, %, mean \pm SD	25 \pm 6	25 \pm 5	24 \pm 6	0.385†

ACE indicates angiotensin-converting enzyme; ARB, angiotensin receptor blocker; CABG, coronary artery bypass graft; CT, computed tomography; EDV, end-diastolic volume; EF, ejection fraction; eGFR, estimated glomerular filtration rate; ESV, end-systolic volume; LBBB, left bundle branch block; NYHA, New York Heart Association; and RV, right ventricle.

**P* value computed using Fisher exact test

†*P* value computed using 2-sample *t* test.

diagram of the subject selection process used in this study. The mean radiation dose across the 82 subjects was 4.4 \pm 2.6 mSv (median, 4.1 mSv; interquartile range, 2 mSv). The baseline characteristics are provided in Table 1.

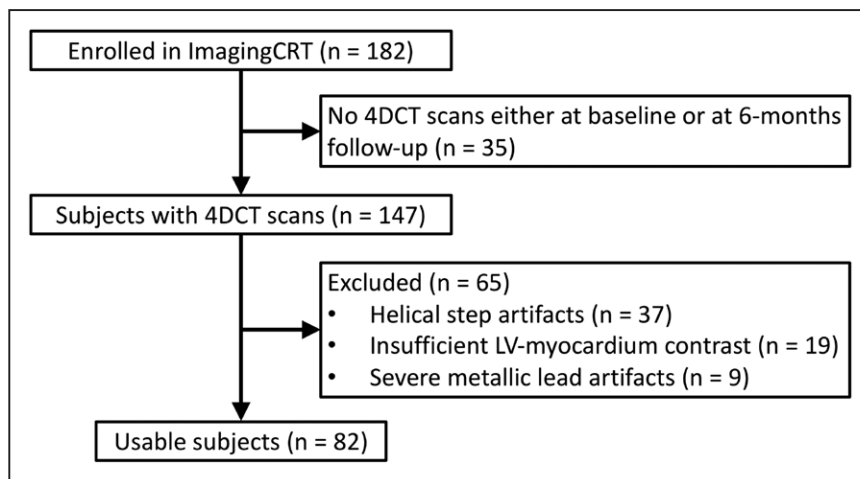


Figure 2. Flow diagram of the subject selection process.

4DCT indicates 4-dimensional computed tomography; ImagingCRT, Empiric Versus Imaging Guided Left Ventricular Lead Placement in Cardiac Resynchronization Therapy trial; and LV, left ventricle.

The CT-derived and the echocardiography-derived LVEFs at baseline were statistically different ($37 \pm 9\%$ versus $25 \pm 6\%$, $P < 0.001$) and poorly correlated ($r = 0.46$, $P < 0.001$).

Lead Placement Score and Response Prediction

Out of the 82 subjects, 52 (63%) had an ESV decrease of $\geq 15\%$ at 6 months follow-up and were considered responders. The average weights of the 12 features used in training the SVM model are shown in Table 2.

Figure 3 shows the relationship between the LPS and the relative change in ESV between the baseline and the

follow-up scans. An LPS threshold of -0.2 maximized the geometric mean (g-mean) value for response prediction; among the subjects above this threshold, the nonresponder rate was 9% ($4/[4+41]$), down from the original nonresponder rate of 37% ($30/82$), and the sensitivity and the specificity at this threshold were 79% and 87%, respectively. The relationship between ΔESV and LPS was statistically significant ($P < 0.001$).

Figure 4A shows the histogram of the LPS values for all 82 subjects. The LPS of the true nonresponders are shown in red while those of the true responders are shown in blue. Figure 4B shows the receiver operating characteristic curve of the prediction model. The area under the curve was 87% (95% CI, 77%–94%). Additionally, the LPS model outperformed a model defined using only clinical predictors of CRT response (see Figure S2).

There is a very practical way to stratify the subjects using the LPS. We can break the subjects into 3 groups with respect to their posttest probabilities: lower probability

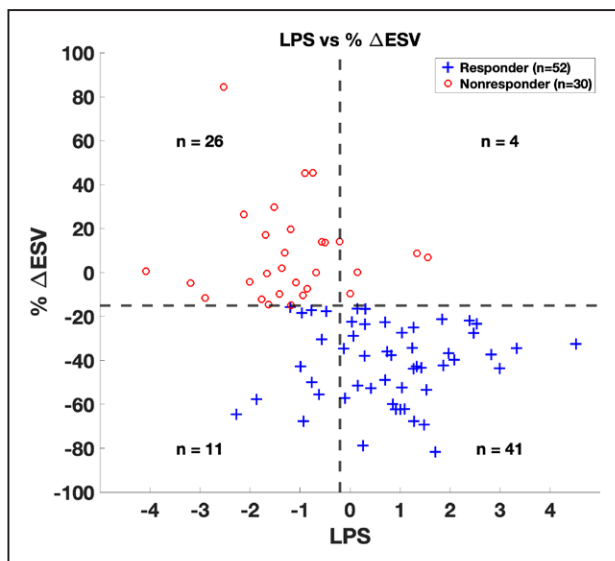


Figure 3. Relationship between change in end-systolic volume (ESV) at 6 months follow-up and lead placement score (LPS).

Distribution of LPS values for the lead locations in each subject as a function of the relative change in ESV between baseline and follow-up scans. The vertical dashed line corresponds to the LPS threshold (-0.2) that maximized the g-mean value for response prediction. The horizontal dashed line corresponds to the response definition of a relative reduction in ESV of 15%. + represents a true responder and o represents a true nonresponder.

Table 2. Feature Weights of the SVM Model With the Responder Criterion Set at $\% \Delta\text{ESV} \leq -15\%$

Feature name	Feature weight for $\% \Delta\text{ESV} \leq -15\%$
1. EDV	0.15
2. ESV	-0.47
3. CURE-SVD	-0.33
4. LVSI	0.22
5. $\text{PRRS}_{\text{Cr-right}}$	0.45
6. $\text{PRRS}_{\text{Cr-left}}$	-0.41
7. $\text{TPRS}_{\text{Cr-right}}$	0.66
8. $\text{TPRS}_{\text{Cr-left}}$	-0.30
9. $\text{MSRS}_{\text{Cr-right}}$	-0.57
10. $\text{MSRS}_{\text{Cr-left}}$	-0.57
11. TOS-right	-0.02
12. TOS-left	1.73

CURE-SVD indicates circumferential uniformity ratio estimate using singular value decomposition; EDV, end-diastolic volume; ESV, end-systolic volume; LVSI, left ventricular sphericity index; MSRS_{Cr} , maximum prestretch of regional shortening; PRRS_{Cr} , peak regional shortening; SVM, support vector machine; TOS, time to onset of shortening; and TPRS_{Cr} , time to peak regional shortening.

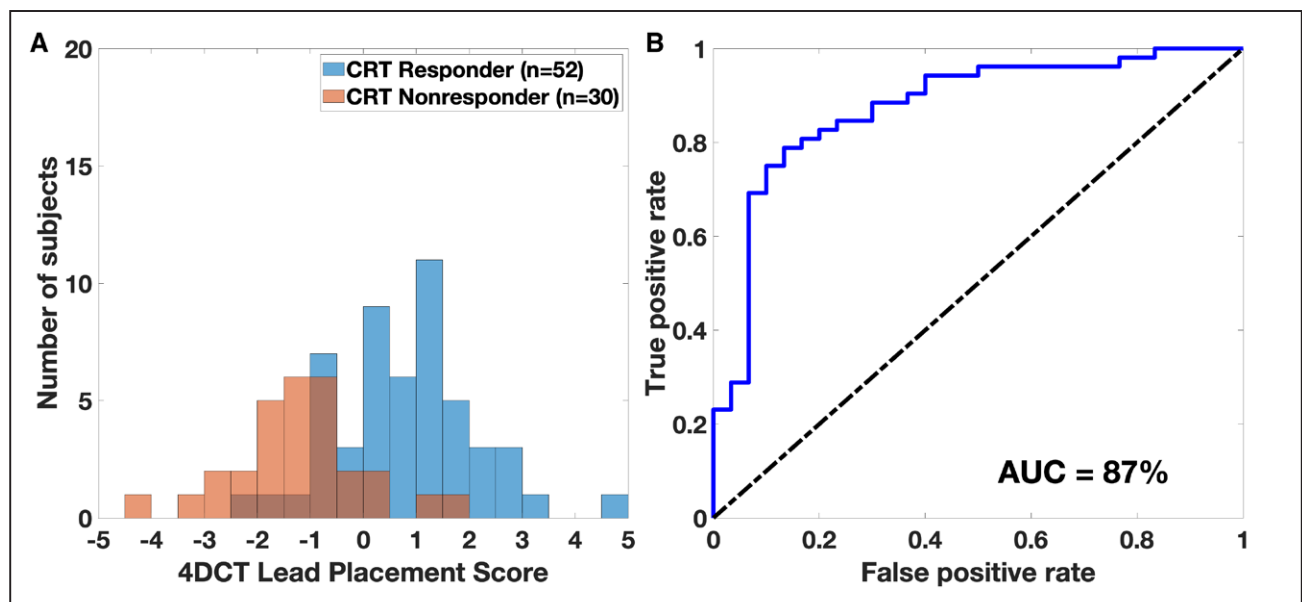


Figure 4. Performance of the trained lead placement score (LPS) model.

A, Histogram of LPS for all 82 subjects. The nonresponders are shown in red, and the responders are shown in blue. **B**, Receiver operating characteristic curve of the trained support vector machine model to predict responders as a function of changing LPS threshold. 4DCT indicates 4-dimensional computed tomography; AUC, area under curve; and CRT, cardiac resynchronization therapy.

of response, unchanged probability, and higher probability of response. Without considering the 4DCT data, the pretest probability of responding to CRT using the $\geq 15\%$ reduction in ESV definition was 52/82 (63%). For the same response definition, by incorporating the 4DCT data, subjects with an LPS in the lowest quartile ($LPS \leq Q_1 = -1$) had a posttest probability of responding of 14% (3/21). Similarly, subjects with an LPS in the highest quartile ($LPS \geq Q_3 = 1.3$) had a posttest probability of responding of 90% (19/21), and for those subjects with an LPS within the interquartile range (interquartile range, $Q_1 < LPS < Q_3$), the posttest probability remained essentially unchanged from the pretest probability (75% versus 63%; $P=0.2$).

Figure 5 shows 4 example subjects that highlight the significance of the LPS in identifying target lead placement sites: (1) a responder ($\% \Delta ESV = -43$) with uniformly high LPS values across the entire LV free wall and the left lead placed in this region of high LPS, (2) a responder ($\% \Delta ESV = -68$) with a localized region of high LPS values on the basal inferolateral wall and the left lead placed in this region of high LPS, (3) a nonresponder ($\% \Delta ESV = -13$) with globally low LPS values and thus the left lead placed in a region of low LPS, and (4) a nonresponder ($\% \Delta ESV = +14$) with a localized region of high LPS values on the basal inferolateral wall, but the left lead not placed in this region of high LPS. For each subject, polar maps of the 4 regional features of LV mechanics (time to onset of shortening, peak regional shortening, time to peak regional shortening, and maximum prestretch of regional shortening) that were used in the derivation of the LPS are shown. Additionally, the

location of the right and the left lead tips are shown by the blue and red highlighted segments, respectively. Also shown are polar maps of the LPS as well as 3-dimensional renderings of the LV lateral wall with the LPS values mapped onto the endocardial surface.

DISCUSSION

The primary objective of this study was to use known quantitative features of LV mechanics derived from baseline 4DCT scans as features in a lead placement score that correlated with CRT response. The main findings reported demonstrate the potential utility of 4DCT in guiding patient selection for CRT; in at least 42 of the 82 subjects used in the study, the LPS could have a significant impact on the decision to proceed with CRT. The study also highlighted the subject-specific variation in the distribution of LPS values across the LV; some subjects had large areas with high LPS values while others had uniformly low LPS values across the LV. Additionally, the interuser and intrauser variability for estimating regional shortening has previously been shown to be very low¹⁹; therefore, the computed LPS values are highly reproducible. Thus, patient-specific LPS maps could aid in the optimal planning and management of patients under consideration for CRT.

CRT Response

Significant effort has been focused on improving the CRT responder rate through the use of imaging and better

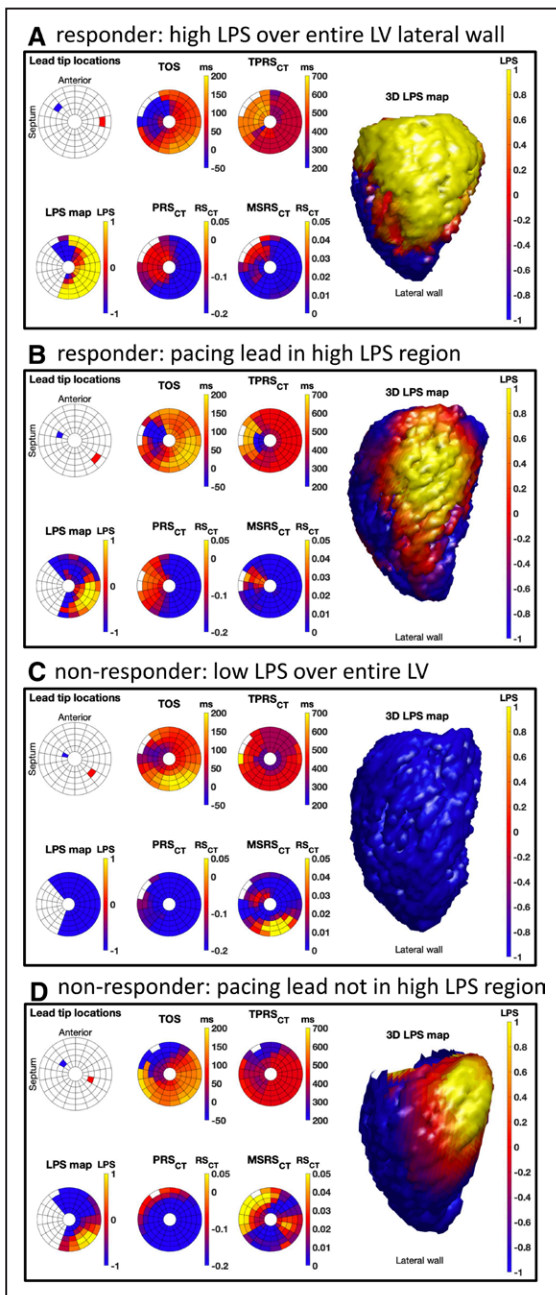


Figure 5. Lead placement score (LPS) maps of cardiac resynchronization therapy responders and nonresponders. **A–D**, Four example subjects with the following information shown for each subject. Lead tip locations: blue=right lead, red=left lead. **A**, A responder ($\% \Delta \text{ESV} = -43$) with uniformly high LPS values across the entire LV free wall and the left lead placed in this region of high LPS. **B**, A responder ($\% \Delta \text{ESV} = -68$) with a localized region of high LPS values on the basal inferolateral wall and the left lead placed in this region of high LPS. **C**, A nonresponder ($\% \Delta \text{ESV} = -13$) with globally low LPS values and thus the left lead placed in a region of low LPS. **D**, A nonresponder ($\% \Delta \text{ESV} = +14$) with a localized region of high LPS values on the basal inferolateral wall, but the left lead not placed in this region of high LPS. 3D LPS map indicates 3-dimensional rendering of the LV lateral wall with LPS values mapped onto the endocardial surface; ESV, end-systolic volume; LPS map, lead placement score map as a polar map; LV, left ventricle; MSRS_{CT}, maximum prestretch of regional shortening; PRS_{CT}, peak regional shortening; TOS, time to onset of shortening, in ms; and TPRS_{CT}, time to peak regional shortening, in ms.

patient selection¹; however, lack of an easily available, robust, and reproducible imaging method coupled with nonconsensus on the definition of CRT response itself have hindered these efforts. Despite 30 years of clinical development, no single definition of CRT response has been universally accepted²²; however, $\geq 15\%$ reduction in LV ESV is the most commonly used^{6,12} and can be measured with great precision using 4DCT. Previous studies using CT to guide CRT have used echocardiography-derived $\% \Delta \text{ESV}$ to determine response^{15,23}; however, the reproducibility of the echocardiography measures is low, causing uncertainty in the results. The image-based response definition used in this study was derived from the LV blood volume segmentations of the baseline and the follow-up 4DCT images, which are highly reproducible²⁴ and are free from any assumptions about LV geometry or manual contouring. For these reasons, we are confident in the precision of the 4DCT-derived measurement of change in ESV as mechanical response. Additionally, the mean baseline CT-derived LVEF was higher than the echocardiography-derived LVEF; this bias was expected as methods of volume estimates derived from CT and echocardiography differ considerably. CT-derived volumes are estimated by simply summing all the segmented LV blood pool voxels, whereas echocardiography-derived volumes are estimated by drawing smooth contours in 2 different imaging planes. Thus, CT-derived volume estimates represent the true 3-dimensional LV blood volume which excludes the volume of the endocardial texture comprising trabecular tissue and papillary muscles, whereas echocardiography-derived volume estimates include the endocardial surface texture volume and papillary muscles.

Support Vector Machine

The 4DCT scans contain an abundance of information; using a limited number of features derived from the scans for training, an SVM model was able to stratify subjects into LV mechanics responders and nonresponders with high accuracy. An SVM was chosen as the desired classifier because (1) it is less susceptible to fitting a model too closely to a specific set of data (overfitting)²⁵ and (2) it has only one optimal solution (no local minima) because it is defined by a convex optimization function (a U-shaped function with only a single lowest point). Due to the limited number of subjects in this study, coupled with the difference in numbers between the responders and the nonresponders (with only 30 nonresponders), it was not feasible to have an independent testing dataset. Thus, we implemented a bagging (bootstrap aggregation)²⁶ approach to overcome this limitation; bagging is an established method that improves stability and helps with overfitting by deriving the final model as an average of all the independent bootstrapped models.²⁷ Despite implementing a bagging approach, the current LPS model needs to be validated using larger independent

testing datasets and prospective clinical trials to derive more robust statistical information on its predictive power as well as to be completely free from overfitting.

Image-Guided CRT

Predicting patient response to CRT with imaging has been extensively researched. Echocardiography, CMR, radionuclide imaging, and CT have all independently shown promise in predicting response.²⁸ Studies using echocardiography,²⁹ single photon emission computed tomography myocardial perfusion imaging,³⁰ CMR,³¹ and CT¹⁶ have all shown a strong correlation between scar burden and CRT nonresponse; the results from our study are concordant with these findings as reflected by the weights of the peak regional shortening feature. Similarly, results from this study agree with previously published work using echo, CMR, and single photon emission computed tomography^{10,29,32} highlighting the strong correlation between pacing at the site of latest mechanical activation and CRT response; the time to onset of shortening-left feature is the most important feature in the LPS model with its feature weight nearly three times that of the second most important feature. Additionally, previous studies have used multimodality imaging to guide CRT including echocardiography, electrocardiography, CMR, CT, fluoroscopy, and single photon emission computed tomography^{18,33}; although beyond the scope of this paper, future studies could investigate developing and optimizing a robust multimodality imaging protocol for comprehensive pre-CRT assessment.

To the best of our knowledge, the influence of maximum prestretch (maximum prestretch of regional shortening) on CRT response has not been previously reported; the results reported in this study reveal it to be a relatively important feature of the model used to stratify subjects for CRT. A large prestretch at either the location of the right or left lead likely detects a region of poor myocardial health which confers the observed reduction in probability of response.

Clinical Utility of LPS

The patient-specific LPS maps could aid in CRT planning and management by providing the clinician with a high-resolution LV map of potential target lead placement sites for achieving a higher probability of CRT response. The results from this study highlight the heterogeneous patient-specific nature of the LPS maps. In patients with large areas of high LPS values, the clinician has multiple target sites for lead placement. In patients with smaller localized regions of high LPS, the clinician needs to find the optimal cardiac vein to reach the target site; if inaccessible, other pacing approaches such as His bundle pacing³⁴ and left bundle branch pacing³⁵ may be considered and more recently leadless endocardial pacing.³⁶

The advantage of 4DCT is that detailed images of the venous anatomy can be obtained³³; hence, the optimal lead delivery approach can be efficiently planned. Lastly, CRT may not be the most effective treatment for patients with uniformly low LPS values across the entire LV, especially since CRT is an invasive procedure and not without risk. Other treatments such as optimal medical therapy, LV assist devices, or heart transplant may be considered for these subjects.

There is some concern with respect to LV lead displacement. To address this, we previously investigated the stability of the pacing leads in the context of lead displacement on the same subject cohort as the one used in this study.³⁷ LV lead displacement was measured as the perpendicular distance from the LV lead tip to the lead body in the relevant coronary sinus between postimplant fluoroscopy and 6 months follow-up cardiac CT. Results from that study demonstrated no significant differences in the measured distances from the lead tips and to the lead bodies between postimplant fluoroscopy and 6 months follow-up cardiac CT ($P=0.84$). Additionally, that study also highlighted the inaccuracy and modest reproducibility of fluoroscopy when compared to cardiac CT for the assessment of LV and right ventricular lead positions.

Four-Dimensional Computed Tomography

Modern 4DCT imaging systems acquire high-resolution images of the entire heart across the full cardiac cycle rapidly, and with wide detector systems (not used in this study), within a single heartbeat. Additionally, images from wide detector scanners do not suffer from step artifacts, enabling artifact-free imaging of patients with arrhythmias. Another benefit of 4DCT is its ability to image patients with implanted metallic medical devices; nearly 28% of CRT candidates have existing right ventricular pacing systems.¹² Additionally, using the dynamic mA feature, the subjects in this study had low CT-based radiation doses (median, 4.1 mSv; interquartile range, 2 mSv), which is comparable to the dose received from natural sources of radiation annually.³⁸ The dose from CT is continuously being reduced as technology advances; from the 2007 and the 2017 dose surveys, the dose from coronary CT angiography was reduced by 78% (885 mGy×cm versus 195 mGy×cm, $P<0.001$).³⁹ New technological advancements such as iterative reconstruction, photon-counting detectors, and the use of deep learning will reduce dose further.⁴⁰

Limitations

This study uses a unique dataset of subjects that had 4DCT scans acquired at both baseline and at 6 months follow-up after CRT implantation, permitting highly precise direct comparisons in LV mechanical states between pre-CRT and post-CRT. Although the models derived in

this study show great promise for using 4DCT in guiding patient selection for CRT, the lack of an independent testing dataset was a limitation. Larger independent testing datasets and prospective trials are needed to ensure generalizability and to understand the true clinical utility and limitations of the LPS model.

The 4DCT images of the 147 subjects used in this study were acquired with a dual-source CT scanner. Due to the limited z axis coverage of the scanner, imaging of the entire superior-inferior extent of the heart was performed in helical mode. Unfortunately, 37 subjects (25%) had severe step artifacts due to beat-to-beat irregularities, rendering the images not usable for dyssynchrony analysis. Despite the excellent temporal resolution of the dual-source scanner (66 ms per frame), wider detector scanners (256 or 320 detector rows) with full heart coverage from a single table position may be better suited for this application, especially with the recent innovations in motion estimation and motion compensation technology.^{41,42}

All 4DCT images used in this study were acquired and reconstructed with the same CT imaging system; this was tremendously advantageous in facilitating a direct comparison of LPS values derived from 4DCT scans of similar image characteristics. However, different scanners yield images of different image quality which could in turn affect the computed LPS values; therefore, to standardize the LPS model across different imaging centers and vendors, future studies will need to explore the sensitivity of the LPS estimates to varying image qualities.

Conclusions

A lead placement score map was developed using features of LV mechanics that were derived from 4DCT images acquired in 82 subjects before CRT implantation. The LPS value at the lead locations correlated with subject response to CRT; LPS effectively reclassified 25% of the subjects into low probability (14%) of response and 25% into high probability (90%) of response, and the remaining 50% of the subjects had a probability of response that was unchanged from the pretest probability (75% versus 63%, $P=0.2$). Additionally, an LPS threshold that maximized the geometric mean of true-negative and true-positive rates categorized subjects as responders and non-responders with high sensitivity (79%) and specificity (87%), with an area under the receiver operating characteristic curve of 87% (95% CI, 77%–94%). These encouraging results highlight the potential utility of 4DCT in planning CRT.

ARTICLE INFORMATION

Received February 28, 2022; accepted July 19, 2022.

Affiliations

Department of Mechanical and Aerospace Engineering (A.M.), Department of Bioengineering (G.M.C., J.Y., Z.C., E.R.M.), Department of Radiology (E.R.M.), and Cardiovascular Division, Department of Medicine (E.R.M.), University of California San Diego, La Jolla. Biomedical Image Technologies Laboratory, ETSI Telecomunicación, Universidad Politécnica de Madrid, Madrid, Spain (M.J.L.-C.). CIBER-BBN, ISCIII, Madrid, Spain (M.J.L.-C.). Department of Cardiology (M.B.K., B.L.N., J.C.N.) and Department of Clinical Medicine (J.C.N.), Aarhus University Hospital, Denmark. Department of Cardiology, Aalborg University Hospital, Denmark (A.S.).

Sources of Funding

This work was supported by grants from the NIH (R01HL144678, F31HL151183, T32HL105373) and the American Heart Association (AHA 20PRE35210261). The ImagingCRT study (Empiric Versus Imaging Guided Left Ventricular Lead Placement in Cardiac Resynchronization Therapy) was funded by Aarhus University, the Danish Heart Foundation (11-04-R84-A3234-22641), the Danish Council for Independent Research (11-107461), Central Denmark Region (1-45-72-4-09), Eva and Henry Frænkels Foundation, and Manufacturer Karl G. Andersens Foundation. Dr Nielsen was supported by a grant from the Novo Nordisk Foundation (NNF16OC0018658).

Disclosures

Dr McVeigh holds founder shares in Clearpoint Neuro Inc and receives research funding from GE Healthcare, Abbott Medical, and Pacesetter Inc. The other authors report no conflicts.

Supplemental Materials

Supplemental Methods

Figures S1 and S2

References 43-50

REFERENCES

1. Prinzen FW, Vernooij K, Auricchio A. Cardiac resynchronization therapy: state-of-the-art of current applications, guidelines, ongoing trials, and areas of controversy. *Circulation*. 2013;128:2407–2418. doi: 10.1161/CIRCULATIONAHA.112.000112
2. Vernooij K, van Deursen CJ, Strik M, Prinzen FW. Strategies to improve cardiac resynchronization therapy. *Nat Rev Cardiol*. 2014;11:481–493. doi: 10.1038/nrcardio.2014.67
3. Marek J, Gandalovičová J, Kejřová E, Pšenička M, Linhart A, Paleček T. Echocardiography and cardiac resynchronization therapy. *Cor et Vasa*. 2016;58:340–351. doi: 10.1016/j.cvasa.2015.08.001
4. Khan FZ, Virdee MS, Palmer CR, Pugh PJ, O'Halloran D, Elvik M, Read PA, Begley D, Fynn SP, Dutka DP. Targeted left ventricular lead placement to guide cardiac resynchronization therapy: the TARGET study: a randomized, controlled trial. *J Am Coll Cardiol*. 2012;59:1509–1518. doi: 10.1016/j.jacc.2011.12.030
5. Vitarelli A, Franciosa P, Rosanio S. Tissue Doppler Imaging in the assessment of selection and response from cardiac resynchronization therapy. *Eur J Echocardiogr*. 2007;8:309–316. doi: 10.1016/j.euje.2006.12.005
6. Chung ES, Leon AR, Tavazzi L, Sun JP, Nihoyannopoulos P, Merlino J, Abraham WT, Ghio S, Leclercq C, Bax JJ, et al. Results of the predictors of response to CRT (PROSPECT) trial. *Circulation*. 2008;117:2608–2616. doi: 10.1161/CIRCULATIONAHA.107.743120
7. Leyva F. Cardiac resynchronization therapy guided by cardiovascular magnetic resonance. *J Cardiovasc Magn Reson*. 2010;12:64. doi: 10.1186/1532-429X-12-64
8. Taylor RJ, Umar F, Panting JR, Stegemann B, Leyva F. Left ventricular lead position, mechanical activation, and myocardial scar in relation to left ventricular reverse remodeling and clinical outcomes after cardiac resynchronization therapy: a feature-tracking and contrast-enhanced cardiovascular magnetic resonance study. *Heart Rhythm*. 2016;13:481–489. doi: 10.1016/j.hrthm.2015.10.024
9. McVeigh ER, Prinzen FW, Wyman BT, Tsitlik JE, Halperin HR, Hunter WC. Imaging asynchronous mechanical activation of the paced heart with tagged MRI. *Magn Reson Med*. 1998;39:507–513. doi: 10.1002/mrm.1910390402
10. Auger DA, Bilchick KC, Gonzalez JA, Cui SX, Holmes JW, Kramer CM, Salerno M, Epstein FH. Imaging left-ventricular mechanical activation in heart failure patients using cine DENSE MRI: validation and implications for cardiac resynchronization therapy. *J Magn Reson Imaging*. 2017;46:887–896. doi: 10.1002/jmri.25613

11. Shetty AK, Duckett SG, Ginks MR, Ma Y, Sohal M, Bostock J, Kapetanakis S, Singh JP, Rhode K, Wright M, et al. Cardiac magnetic resonance-derived anatomy, scar, and dyssynchrony fused with fluoroscopy to guide LV lead placement in cardiac resynchronization therapy: a comparison with acute haemodynamic measures and echocardiographic reverse remodelling. *Eur Heart J Cardiovasc Imaging*. 2013;14:692–699. doi: 10.1093/ehjci/jes270
12. Daubert JC, Saxon L, Adamson PB, Auricchio A, Berger RD, Beshai JF, Breithard O, Brignole M, Cleland J, DeLurgio DB, et al. 2012 EHRA/HRS expert consensus statement on cardiac resynchronization therapy in heart failure: implant and follow-up recommendations and management: a registered branch of the European Society of Cardiology (ESC), and the Heart Rhythm Society; and in col. *Europace*. 2012;14:1236–1286. doi: 10.1093/europace/eus222
13. Truong QA, Szymonifka J, Picard MH, Thai WE, Wai B, Cheung JW, Heist EK, Hoffmann U, Singh JP. Utility of dual-source computed tomography in cardiac resynchronization therapy-DIRECT study. *Heart Rhythm*. 2018;15:1206–1213. doi: 10.1016/j.hrthm.2018.03.020
14. Behar JM, Rajani R, Pourmorteza A, Preston R, Razeghi O, Niederer S, Adhya S, Claridge S, Jackson T, Sieniewicz B, et al. Comprehensive use of cardiac computed tomography to guide left ventricular lead placement in cardiac resynchronization therapy. *Heart Rhythm*. 2017;14:1364–1372. doi: 10.1016/j.hrthm.2017.04.041
15. Gould J, Sidhu BS, Sieniewicz BJ, Porter B, Lee AWC, Razeghi O, Behar JM, Mehta V, Elliott MK, Toth D, et al. Feasibility of intraprocedural integration of cardiac CT to guide left ventricular lead implantation for CRT upgrades. *J Cardiovasc Electrophysiol*. 2021;32:802–812. doi: 10.1111/jce.14896
16. Fyenbo DB, Sommer A, Kühl JT, Kofoed KF, Nørgaard BL, Kronborg MB, Bouchelouche K, Nielsen JC. Transmural myocardial scar assessed by cardiac computed tomography: predictor of echocardiographic versus clinical response to cardiac resynchronization therapy? *J Comput Assist Tomogr*. 2019;43:312–316. doi: 10.1097/RCT.0000000000000824
17. Sommer A, Kronborg MB, Poulsen SH, Böttcher M, Nørgaard BL, Bouchelouche K, Mortensen PT, Gerdes C, Nielsen JC. Empiric versus imaging guided left ventricular lead placement in cardiac resynchronization therapy (ImagingCRT): study protocol for a randomized controlled trial. *Trials*. 2013;14:113. doi: 10.1186/1745-6215-14-113
18. Sommer A, Kronborg MB, Nørgaard BL, Poulsen SH, Bouchelouche K, Böttcher M, Jensen HK, Jensen JM, Kristensen J, Gerdes C, et al. Multimodality imaging-guided left ventricular lead placement in cardiac resynchronization therapy: a randomized controlled trial. *Eur J Heart Fail*. 2016;18:1365–1374. doi: 10.1002/ehf.530
19. Colvert GM, Manohar A, Contijoch FJ, Yang J, Glynn J, Blanke P, Leipsic JA, McVeigh ER. Novel 4DCT method to measure regional left ventricular endocardial shortening before and after transcatheter mitral valve implantation. *Struct Heart*. 2021;5:410–419. doi: 10.1080/24748706.2021.1934617
20. Manohar A, Colvert GM, Schluchter A, Contijoch F, McVeigh ER. Anthropomorphic left ventricular mesh phantom: a framework to investigate the accuracy of SQUEEZ using Coherent Point Drift for the detection of regional wall motion abnormalities. *J Med Imaging (Bellingham)*. 2019;6:045001. doi: 10.1117/1.JMI.6.4.045001
21. Feeny AK, Rickard J, Patel D, Toro S, Trulock KM, Park CJ, LaBarbera MA, Varma N, Niebauer MJ, Sinha S, et al. Machine learning prediction of response to cardiac resynchronization therapy: improvement versus current guidelines. *Circ Arrhythm Electrophysiol*. 2019;12:e007316. doi: 10.1161/CIRCEP.119.007316
22. Daubert C, Behar N, Martins RP, Mabo P, Leclercq C. Avoiding non-responders to cardiac resynchronization therapy: a practical guide. *Eur Heart J*. 2017;38:1463–1472. doi: 10.1093/eurheartj/ehw270
23. Kronborg MB, Sommer A, Fyenbo DB, Nørgaard BL, Gerdes C, Jensen JM, Jensen HK, Kristensen J, Nielsen JC. Left ventricular regional remodeling and lead position during cardiac resynchronization therapy. *Heart Rhythm*. 2018;15:1542–1549. doi: 10.1016/j.hrthm.2018.04.012
24. Sugeng L, Mor-Avi V, Weinert L, Niel J, Ebner C, Steringer-Mascherbauer R, Schmidt F, Galuschky C, Schummers G, Lang RM, et al. Quantitative assessment of left ventricular size and function: side-by-side comparison of real-time three-dimensional echocardiography and computed tomography with magnetic resonance reference. *Circulation*. 2006;114:654–661. doi: 10.1161/CIRCULATIONAHA.106.626143
25. Cortes C, Vapnik V. Support-vector networks. *Machine Learning*. 1995;20:273–297. doi: 10.1007/BF00994018
26. Bauer E, Kohavi R. Empirical comparison of voting classification algorithms: bagging, boosting, and variants. *Machine Learning*. 1999;36:105–139.
27. Sukhanov S, Merentitis A, Debes C, Hahn J, Zoubir AM. Bootstrap-based SVM aggregation for class imbalance problems. In: 2015 23rd European Signal Processing Conference (EUSIPCO). IEEE; 2015:165–169.
28. Heydari B, Jerosch-Herold M, Kwong RY. Imaging for planning of cardiac resynchronization therapy. *JACC Cardiovasc Imaging*. 2012;5:93–110. doi: 10.1016/j.jcmg.2011.11.006
29. Delgado V, van Bommel RJ, Bertini M, Borleffs CJ, Marsan NA, Arnold CT, Nucifora G, van de Veire NR, Ypenburg C, Boersma E, et al. Relative merits of left ventricular dyssynchrony, left ventricular lead position, and myocardial scar to predict long-term survival of ischemic heart failure patients undergoing cardiac resynchronization therapy. *Circulation*. 2011;123:70–78. doi: 10.1161/CIRCULATIONAHA.110.945345
30. Xu YZ, Cha YM, Feng D, Powell BD, Wiste HJ, Hua W, Chareonthaitawee P. Impact of myocardial scarring on outcomes of cardiac resynchronization therapy: extent or location? *J Nucl Med*. 2012;53:47–54. doi: 10.2967/jnumed.111.095448
31. Chalil S, Foley PW, Muhyaldeen SA, Patel KC, Yousef ZR, Smith RE, Frenneaux MP, Leyva F. Late gadolinium enhancement-cardiovascular magnetic resonance as a predictor of response to cardiac resynchronization therapy in patients with ischaemic cardiomyopathy. *Europace*. 2007;9:1031–1037. doi: 10.1093/europace/eum133
32. Boogers MJ, Chen J, van Bommel RJ, Borleffs CJ, Dibbets-Schneider P, van der Hiel B, Al Younis I, Schalij MJ, van der Wall EE, Garcia EV, et al. Optimal left ventricular lead position assessed with phase analysis on gated myocardial perfusion SPECT. *Eur J Nucl Med Mol Imaging*. 2011;38:230–238. doi: 10.1007/s00259-010-1621-z
33. Nguyễn UC, Cluitmans MJM, Strik M, Luermans JG, Gommers S, Wildberger JE, Bekkers SCAM, Volders PGA, Muhl C, Prinzen FW, et al. Integration of cardiac magnetic resonance imaging, electrocardiographic imaging, and coronary venous computed tomography angiography for guidance of left ventricular lead positioning. *Europace*. 2019;21:626–635. doi: 10.1093/europace/euy292
34. Lewis AJM, Foley P, Whinnett Z, Keene D, Chandrasekaran B. His bundle pacing: a new strategy for physiological ventricular activation. *J Am Heart Assoc*. 2019;8:e010972. doi: 10.1161/JAHA.118.010972
35. Huang W, Chen X, Su L, Wu S, Xia X, Vijayaraman P. A beginner's guide to permanent left bundle branch pacing. *Heart Rhythm*. 2019;16:1791–1796. doi: 10.1016/j.hrthm.2019.06.016
36. Galand V, Singh JP, Leclercq C. Alternative left ventricular pacing approaches for optimal cardiac resynchronization therapy. *Heart Rhythm*. 2019;16:1281–1289. doi: 10.1016/j.hrthm.2019.03.011
37. Sommer A, Kronborg MB, Nørgaard BL, Gerdes C, Mortensen PT, Nielsen JC. Left and right ventricular lead positions are imprecisely determined by fluoroscopy in cardiac resynchronization therapy: a comparison with cardiac computed tomography. *Europace*. 2014;16:1334–1341. doi: 10.1093/europace/euu056
38. McCollough CH, Primak AN, Braun N, Kofler J, Yu L, Christner J. Strategies for reducing radiation dose in CT. *Radiol Clin North Am*. 2009;47:27–40. doi: 10.1016/j.rcl.2008.10.006
39. Stocker TJ, Deseive S, Leipsic J, Hadamitzky M, Chen MY, Rubinshtein R, Heckner M, Bax JJ, Fang XM, Grove EL, et al; PROTECTION VI investigators. Reduction in radiation exposure in cardiovascular computed tomography imaging: results from the PROspective multicenter registry on radiation dose Estimates of cardiac CT angiography in daily practice in 2017 (PROTECTION VI). *Eur Heart J*. 2018;39:3715–3723. doi: 10.1093/eurheartj/ehy546
40. Lell MM, Kachelrieß M. Recent and upcoming technological developments in computed tomography: high speed, low dose, deep learning, multienergy. *Invest Radiol*. 2020;55:8–19. doi: 10.1097/RLI.0000000000000601
41. Pack JD, Manohar A, Ramani S, Claus B, Yin Z, Contijoch FJ, Schluchter AJ, McVeigh ER. Four-dimensional computed tomography of the left ventricle, part I: motion artifact reduction. *Med Phys*. 2022;49:4404–4418. doi: 10.1002/mp.15709
42. Manohar A, Pack JD, Schluchter AJ, McVeigh ER. Four-dimensional computed tomography of the left ventricle, part II: estimation of mechanical activation times. *Med Phys*. 2022;49:2309–2323. doi: 10.1002/mp.15550
43. Leclercq C, Faris O, Tunin R, Johnson J, Kato R, Evans F, Spinelli J, Halperin H, McVeigh E, Kass DA. Systolic improvement and mechanical resynchronization does not require electrical synchrony in the dilated failing heart with left bundle-branch block. *Circulation*. 2002;106:1760–1763. doi: 10.1161/01.cir.0000035037.11968.5c
44. Ramachandran R, Chen X, Kramer CM, Epstein FH, Bilchick KC. Singular value decomposition applied to cardiac strain from mr imaging for

- selection of optimal cardiac resynchronization therapy candidates. *Radiology*. 2015;275:413–420. doi: 10.1148/radiol.14141578
45. Ambale-Venkatesh B, Yoneyama K, Sharma RK, Ohyama Y, Wu CO, Burke GL, Shea S, Gomes AS, Young AA, Bluemke DA, et al. Left ventricular shape predicts different types of cardiovascular events in the general population. *Heart*. 2017;103:499–507. doi: 10.1136/heartjnl-2016-310052
46. Wyman BT, Hunter WC, Prinzen FW, McVeigh ER. Mapping propagation of mechanical activation in the paced heart with MRI tagging. *Am J Physiol*. 1999;276:H881–H891. doi: 10.1152/ajpheart.1999.276.3.H881
47. Wyman BT, Hunter WC, Prinzen FW, Faris OP, McVeigh ER. Effects of single- and biventricular pacing on temporal and spatial dynamics of ventricular contraction. *Am J Physiol Heart Circ Physiol*. 2002;282:H372–H379. doi: 10.1152/ajpheart.2002.282.1.H372
48. He H, Ma Y. *Imbalanced Learning: Foundations, Algorithms, and Applications*. (He H, Ma Y, eds.). Wiley; 2013.
49. Donders AR, van der Heijden GJ, Stijnen T, Moons KG. Review: a gentle introduction to imputation of missing values. *J Clin Epidemiol*. 2006;59:1087–1091. doi: 10.1016/j.jclinepi.2006.01.014
50. Lin WJ, Chen JJ. Class-imbalanced classifiers for high-dimensional data. *Brief Bioinform*. 2013;14:13–26. doi: 10.1093/bib/bbs006